Wei Gao, Ruizhong Hu, Xueyun Wang, Runsheng Yin, Xianwu Bi, Zhuojun, Xie, Shanling Fu, and Jun Yan, 2022, Large-scale basement mobilization endows the giant Carlin-type gold mineralization in the Youjiang Basin, South China: Insights from mercury isotopes: GSA Bulletin, https://doi.org/10.1130/B36636.1.

Supplemental Material

Text S1. Mercury isotopic composition of terrestrial and marine reservoirs.

Figure S1. Plots of δ^{202}Hg versus Δ^{199}Hg (a), and Δ^{201}Hg versus Δ^{199}Hg (b) of terrestrial and marine reservoirs.

Text S2. Two endmember mixing model of mercury isotope.

Table S1. Descriptions of the Precambrian basement rocks collected in this study from the periphery the Youjiang basin of South China.

Table S2. THg and Hg isotopic compositions of ore-associated sulfides of the Carlin-type gold deposits in the Youjiang basin of South China.

Table S3. THg and Hg isotopic compositions of Precambrian basement rocks from the periphery of the Youjiang basin, respectively.

Table S4. THg and Hg isotopic compositions of the Permian E'meishan plume-related mafic rocks from the interior of the Youjiang basin, respectively.

TEXT S1. MERCURY ISOTOPIC COMPOSITION OF TERRESTRIAL AND MARINE RESERVOIRS

The data defining the Hg isotopic composition of terrestrial and marine reservoirs are sourced from literature. The data of terrestrial soils were from Biswas et al. (2008), Estrade et al. (2010), and Zhang et al. (2013). Data of terrestrial soil and sediments affected by mercury mining have been excluded. The data of marine sediments were from Gehrke et al. (2009), Yin et al. (2015) and Meng et al. (2019). We have tried our best to eliminate the data of samples collected from coastal and shelf areas, which receive Hg from terrestrial soil runoff.

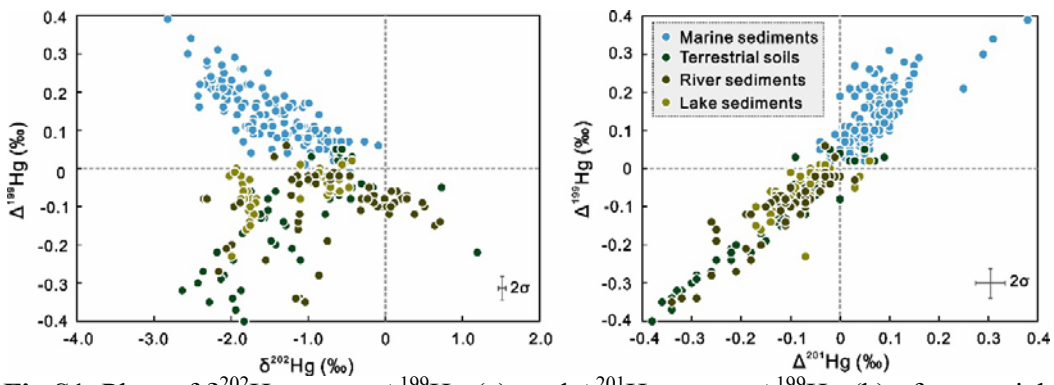

Fig S1. Plots of δ^{202}Hg versus Δ^{199}Hg (a), and Δ^{201}Hg versus Δ^{199}Hg (b) of terrestrial and marine reservoirs.

TEXT S2. TWO ENDMEMBER MIXING MODEL OF MERCURY ISOTOPE

To quantify the contribution fraction of basement rocks and magmatic-hydrothermal system, we built two-endmember isotope mixing model:

$$f_b + f_m = 1$$

$$f_b \times \Delta^{199}Hg_b + f_m \times \Delta^{199}Hg_m = \Delta^{199}Hg_S$$

where f_b and f_m are the fractional contributions of basement rocks and magmatic system, respectively. $\Delta^{199}Hg_b$, $\Delta^{199}Hg_m$ and $\Delta^{199}Hg_S$ are the mean isotopic values of basement rocks, magmatic system and ore-associated sulfides obtained in this study, respectively.

The model calculation was accomplished by the R programming language. The Monte Carlo simulation was performed to quantify mean results and uncertainties of the model. Given such modeling techniques relies on random sampling and statistical data analysis, Monte Carlo simulation was applied on explore the potential results and its density in 100 thousand simulations with normal distribution (around 1σ) random variation isotopic signatures in Rstudio.

Table S1. Descriptions of the Precambrian basement rocks collected in this study from the periphery the Youjiang basin of South China

Sample	Lithology	Strata	Era
fjs-2	Sandstone	Nantuo Formation, Cryogenian	Cryogenian
sd-5	Siltstone	Nantuo Formation, Cryogenian	Cryogenian
tz-801	Siltstone	Nantuo Formation, Cryogenian	Cryogenian
fjs-8	Silty mudstone	Nantuo Formation, Cryogenian	Cryogenian
tz-03	Slate	Qingshuijiang Formation, Banxi Group	Late Tonian
fjs-701	Slate	Qingshuijiang Formation, Banxi Group	Late Tonian
fjs-9	Siltstone	Fanzhao Formation, Banxi Group	Late Tonian
tz-18	Slate	Fanzhao Formation, Banxi Group	Late Tonian
tz-21	Slate	Wuye Formation, Banxi Group	Late Tonian
fjs-11-1	Siltstone	Wuye Formation, Banxi Group	Late Tonian
fjs-18	Slate	Waxi formation, Fanjingshan Group	Middle Tonian
fjs-16	Sandstone	Tongchang Formation, Fanjingshan Group	Middle Tonian
fjs-1502	Slate	Huixiangping formation, Fanjingshan Group	Middle Tonian
fjs-15	Slate	Huixiangping formation, Fanjingshan Group	Middle Tonian
fjs-17	Slate	Xiaojiahe formation, Fanjingshan Group	Middle Tonian
fjs-21	Siltstone	Yujiagou formation, Fanjingshan Group	Middle Tonian

Table S2. THg and Hg isotopic compositions of ore-associated sulfides of the Carlin-type gold deposits in the Youjiang basin of South China

Sample	Type	THg	δ^{202}Hg	δ^{201}Hg	δ^{200}Hg	δ^{199}Hg	Δ^{201}Hg	Δ^{200}Hg	Δ^{199}Hg
ID		ppm	‰	‰	‰	‰	‰	‰	‰
Shuiyindong Au deposit									
SYD-1	Pyrite	49.4	0.49	0.44	0.38	0.06	0.07	0.13	-0.07
SYD-2	Pyrite	40.3	0.36	0.26	0.27	0.00	-0.02	0.09	-0.09
SYD-3	Pyrite	29.0	-0.05	-0.28	-0.11	-0.12	-0.24	-0.09	-0.11
SYD-4	Pyrite	32.6	-0.05	-0.20	-0.10	-0.11	-0.16	-0.07	-0.09
SYD-5	Pyrite	18.4	-0.16	-0.17	-0.11	-0.16	-0.05	-0.03	-0.12
SYD-6	Pyrite	20.2	0.70	0.43	0.33	0.00	-0.10	-0.02	-0.17
SYD-7	Pyrite	4.32	0.09	0.14	0.19	0.00	0.07	0.15	-0.03
SYD-8	Pyrite	3.34	0.29	0.06	0.09	-0.08	-0.16	-0.06	-0.16
SYD-9	Realgar	2.30	0.24	0.18	0.14	0.00	0.00	0.02	-0.06
SYD-10	Realgar	1.26	-1.61	-1.29	-0.87	-0.47	-0.08	-0.07	-0.07
SYD-11	Stibnite	130	-1.05	-0.86	-0.54	-0.32	-0.08	-0.02	-0.06
SYD-12	Stibnite	85.3	-1.26	-1.01	-0.56	-0.35	-0.06	0.07	-0.03
SYD-13	Stibnite	1.36	-0.10	-0.17	-0.05	-0.10	-0.10	0.00	-0.08
Jinfeng-Linwang Au deposits									
LNG-1	Pyrite	32.5	-0.32	-0.35	-0.21	-0.14	-0.11	-0.05	-0.06
LNG-2	Pyrite	18.6	0.26	0.10	0.10	-0.07	-0.10	-0.03	-0.14
LNG-3	Pyrite	10.4	-0.45	-0.47	-0.22	-0.16	-0.13	0.01	-0.05
LNG-4	Pyrite	25.8	0.52	0.33	0.29	0.11	-0.06	0.03	-0.02
LNG-5	Pyrite	15.8	0.27	0.10	0.09	-0.09	-0.10	-0.05	-0.16
LNG-6	Pyrite	42.1	-0.39	-0.31	-0.17	-0.13	-0.01	0.03	-0.03
LNG-7	Stibnite	1302	-0.08	-0.10	-0.05	-0.05	-0.04	-0.01	-0.03
LNG-8	Stibnite	1324	-0.17	-0.17	-0.08	-0.06	-0.04	0.01	-0.02
LNG-9	Stibnite	88.8	-0.01	-0.14	-0.01	-0.03	-0.13	0.00	-0.03
LNG-10	Orpiment	0.89	-1.07	-0.82	-0.56	-0.32	-0.02	-0.02	-0.05
LNG-11	Orpiment	4.65	-1.03	-0.78	-0.55	-0.22	-0.01	-0.03	0.04
LW1	Pyrite	33.2	1.21	0.79	0.60	0.17	-0.12	0.00	-0.13
LW2	Pyrite	42.6	0.88	0.57	0.43	0.03	-0.09	-0.01	-0.19
LW3	Pyrite	56.8	3.26	2.28	1.63	0.53	-0.17	-0.01	-0.29
LW4	Pyrite	63.9	0.64	0.37	0.37	0.06	-0.11	0.05	-0.10
LW5	Pyrite	4.74	0.76	0.44	0.29	-0.05	-0.13	-0.10	-0.24
LW7	Pyrite	16.6	0.93	0.59	0.41	-0.01	-0.11	-0.06	-0.24
LW8	Pyrite	2.49	0.20	0.09	0.16	0.01	-0.05	0.06	-0.04
LW9	Pyrite	2.49	0.21	0.15	0.12	-0.07	-0.01	0.02	-0.13
LW10	Pyrite	10.2	0.86	0.56	0.47	0.16	-0.09	0.04	-0.06
LW11	Pyrite	5.76	0.92	0.48	0.34	-0.02	-0.21	-0.12	-0.25
Jinya-Nakuang Au deposits									

JY-1	Pyrite	3.68	0.30	0.14	0.19	-0.08	-0.08	0.04	-0.15
JY-2	Pyrite	4.72	0.48	0.25	0.24	-0.04	-0.12	0.00	-0.16
JY-3	Pyrite	3.52	0.46	0.25	0.24	-0.06	-0.10	0.01	-0.18
JY-4	Pyrite	1.33	0.36	0.03	0.08	-0.18	-0.24	-0.10	-0.27
JY-5	Arsenopyrite	3.15	0.38	0.17	0.16	-0.07	-0.12	-0.03	-0.16
JY-6	Arsenopyrite	3.87	0.60	0.31	0.26	-0.04	-0.14	-0.05	-0.19
JY-7	Arsenopyrite	3.99	-0.61	-0.53	-0.32	-0.33	-0.08	-0.02	-0.18
JY-8	Arsenopyrite	4.32	-0.55	-0.47	-0.25	-0.15	-0.06	0.02	-0.01
NK-1	Arsenopyrite	0.65	-0.07	-0.04	0.02	-0.16	0.01	0.06	-0.14
NK-2	Arsenopyrite	0.48	-0.02	-0.01	0.04	-0.04	0.01	0.05	-0.04
NK-3	Arsenopyrite	0.65	-0.82	-0.60	-0.40	-0.38	0.02	0.01	-0.17
NK-4	Arsenopyrite	1.29	0.11	-0.01	0.10	-0.12	-0.09	0.05	-0.15
NK-5	Arsenopyrite	0.47	0.18	0.10	0.16	-0.06	-0.04	0.07	-0.10
NK-6	Arsenopyrite	0.45	-0.29	-0.34	-0.20	-0.25	-0.13	-0.06	-0.18
NK-7	Pyrite	1.13	-0.45	-0.30	-0.26	-0.27	0.04	-0.03	-0.15
NK-8	Pyrite	0.77	0.31	0.17	0.21	-0.11	-0.06	0.06	-0.19
NK-9	Pyrite	1.74	0.19	0.04	0.04	-0.10	-0.10	-0.06	-0.14
NK-10	Pyrite	0.83	0.27	0.18	0.23	0.04	-0.03	0.09	-0.03
Badu Au deposit									
BD-1	Pyrite	0.13	0.39	0.20	0.07	-0.14	-0.09	-0.13	-0.24
BD-2	Pyrite	2.13	0.10	-0.14	-0.12	-0.20	-0.21	-0.17	-0.23
BD-3	Pyrite	0.57	0.09	-0.18	-0.08	-0.14	-0.24	-0.12	-0.17
BD-4	Pyrite	0.46	0.20	0.05	0.10	0.02	-0.10	0.00	-0.03
BD-5	Pyrite	0.56	0.20	0.06	0.10	-0.01	-0.09	0.01	-0.06
BD-6	Pyrite	1.33	-0.61	-0.40	-0.29	-0.14	0.06	0.01	0.02
BD-7	Pyrite	0.66	0.18	0.09	0.09	-0.06	-0.05	0.00	-0.11
BD-8	Pyrite	0.58	-0.30	-0.28	-0.16	-0.12	-0.06	-0.01	-0.04
BD-9	Pyrite	1.32	-0.52	-0.43	-0.29	-0.22	-0.03	-0.02	-0.09
BD-10	Pyrite	1.01	0.04	-0.03	0.03	-0.11	-0.06	0.01	-0.12
BD-11	Pyrite	17.08	0.86	0.44	0.39	0.04	-0.20	-0.05	-0.18
BD-13	Pyrite	1.38	0.60	0.28	0.25	-0.05	-0.17	-0.05	-0.20
BD-15	Pyrite	0.59	1.20	0.74	0.54	0.12	-0.16	-0.06	-0.18
BD-16	Arsenopyrite	1.07	-0.29	-0.23	-0.08	-0.11	-0.01	0.07	-0.04
BD-17	Arsenopyrite	0.32	0.03	-0.11	-0.02	-0.14	-0.13	-0.03	-0.15
BD-18	Arsenopyrite	1.32	-0.82	-0.58	-0.41	-0.33	0.03	0.00	-0.12
BD-19	Stibnite	0.79	0.25	0.12	0.17	-0.01	-0.06	0.04	-0.08
BD-20	Stibnite	0.96	-0.26	-0.25	-0.13	-0.06	-0.05	0.00	0.00
BD-21	Stibnite	0.59	0.12	-0.01	0.03	-0.06	-0.10	-0.03	-0.10
BD-22	Stibnite	0.64	0.61	0.28	0.26	-0.02	-0.18	-0.05	-0.18
BD-23	Stibnite	1.12	0.00	-0.12	-0.04	-0.10	-0.12	-0.04	-0.10
BD-24	Stibnite	1.09	1.02	0.75	0.58	0.08	-0.01	0.07	-0.17
Lanmuchang Hg-Au deposit									
lmc-1	Cinnabar	--	0.48	0.24	0.23	0.01	-0.12	-0.01	-0.11
lmc-2	Cinnabar	--	-0.14	-0.15	-0.06	-0.06	-0.05	0.01	-0.03

lmc-3	Cinnabar	--	-0.01	-0.07	0.05	-0.05	-0.06	0.06	-0.05
lmc-4	Cinnabar	--	-0.13	-0.21	-0.07	-0.09	-0.11	-0.01	-0.06
lmc-5	Cinnabar	--	-0.52	-0.46	-0.25	-0.16	-0.07	0.01	-0.03
lmc-6	Cinnabar	--	-0.23	-0.25	-0.14	-0.15	-0.08	-0.02	-0.09
lmc-7	Cinnabar	--	-0.24	-0.30	-0.15	-0.12	-0.12	-0.03	-0.06
lmc-8	Cinnabar	--	0.16	0.03	0.07	-0.05	-0.09	-0.01	-0.09
lmc-9	Cinnabar	--	-0.26	-0.25	-0.11	-0.12	-0.05	0.03	-0.05
lmc-10	Cinnabar	--	-0.14	-0.18	-0.10	-0.14	-0.07	-0.03	-0.10
lmc-11	Cinnabar	--	-0.01	-0.07	0.00	-0.02	-0.07	0.00	-0.02
lmc-12	Cinnabar	--	0.50	0.26	0.28	-0.01	-0.11	0.03	-0.13
lmc-13	Cinnabar	--	-0.39	-0.40	-0.20	-0.17	-0.10	0.00	-0.07
lmc-14	Cinnabar	--	-0.22	-0.21	-0.10	-0.09	-0.05	0.01	-0.04
lmc-15	Cinnabar	--	0.38	0.16	0.16	0.04	-0.13	-0.03	-0.05
lmc-16	Cinnabar	--	0.33	0.13	0.15	-0.02	-0.12	-0.01	-0.10
lmc-17	Cinnabar	--	0.15	0.05	0.07	0.00	-0.07	-0.01	-0.04
lmc-18	Cinnabar	--	-0.50	-0.40	-0.27	-0.14	-0.02	-0.02	-0.02
lmc-19	Cinnabar	--	-0.46	-0.35	-0.23	-0.15	-0.01	0.00	-0.03
lmc-20	Cinnabar	--	-0.30	-0.21	-0.13	-0.09	0.01	0.02	-0.01
lmc-21	Cinnabar	--	0.72	0.49	0.37	0.12	-0.06	0.01	-0.06
lmc-22	Cinnabar	--	0.06	-0.05	0.03	-0.09	-0.09	0.00	-0.10
lmc-23	Cinnabar	--	0.08	0.02	0.04	0.00	-0.05	0.00	-0.02
lmc-24	Cinnabar	--	0.35	0.16	0.13	-0.03	-0.11	-0.05	-0.12
lmc-25	Cinnabar	--	-0.04	-0.10	-0.03	-0.04	-0.07	-0.01	-0.03
NIST-3177 secondary Hg standard solution									
3177-1	--	--	-0.48	-0.39	-0.25	-0.15	-0.04	-0.02	-0.03
3177-2	--	--	-0.53	-0.43	-0.26	-0.14	-0.04	0.00	0.00
3177-3	--	--	-0.47	-0.39	-0.26	-0.13	-0.04	-0.02	-0.01
3177-4	--	--	-0.55	-0.45	-0.30	-0.14	-0.04	-0.02	0.00
3177-5	--	--	-0.45	-0.37	-0.22	-0.13	-0.03	0.00	-0.02
3177-6	--	--	-0.49	-0.41	-0.28	-0.16	-0.05	-0.04	-0.04
3177-7	--	--	-0.46	-0.40	-0.21	-0.11	-0.06	0.02	0.01
3177-8	--	--	-0.48	-0.39	-0.27	-0.12	-0.03	-0.03	0.00
3177-9	--	--	-0.47	-0.38	-0.17	-0.15	-0.03	0.06	-0.04
3177-10	--	--	-0.58	-0.42	-0.29	-0.16	0.02	0.00	-0.01
3177-11	--	--	-0.59	-0.43	-0.26	-0.09	0.02	0.03	0.06
GSS-4 soil standard reference material									
GSS-4(1)	--	--	-1.74	-1.73	-0.87	-0.89	-0.42	0.00	-0.45
GSS-4(2)	--	--	-1.72	-1.70	-0.90	-0.86	-0.41	-0.03	-0.42
GSS-4(3)	--	--	-1.85	-1.79	-0.94	-0.85	-0.41	-0.02	-0.38
GSS-4(4)	--	--	-1.75	-1.68	-0.85	-0.81	-0.36	0.02	-0.37
GSS-4(5)	--	--	-1.85	-1.82	-0.92	-0.84	-0.43	0.01	-0.38

Table S3. THg and Hg isotopic compositions of Precambrian basement rocks from the periphery of the Youjiang basin, respectively.

Sample	Type	THg	δ^{202}Hg	δ^{201}Hg	δ^{200}Hg	δ^{199}Hg	Δ^{201}Hg	Δ^{200}Hg	Δ^{199}Hg
ID		ppb	‰	‰	‰	‰	‰	‰	‰
fjs-2	Sandstone	20	-0.86	-0.71	-0.42	-0.22	-0.06	0.01	-0.01
sd-5	Siltstone	52	-0.75	-0.60	-0.36	-0.18	-0.03	0.02	0.01
tz-801	Siltstone	39	1.66	1.13	0.83	0.33	-0.12	0.00	-0.08
fjs-8	Silty mudstone	33	-0.79	-0.58	-0.32	-0.16	0.02	0.08	0.04
tz-03	Slate	46	-1.25	-1.03	-0.63	-0.37	-0.09	0.00	-0.05
fjs-701	Slate	58	-0.56	-0.40	-0.32	-0.09	0.03	-0.04	0.05
fjs-9	Siltstone	58	-0.84	-0.59	-0.38	-0.22	0.04	0.04	0.00
tz-18	Slate	32	0.57	0.42	0.32	0.02	-0.01	0.03	-0.12
tz-21	Slate	23	0.19	0.02	0.03	-0.09	-0.12	-0.07	-0.14
fjs-11-1	Siltstone	60	1.40	0.89	0.70	0.24	-0.16	0.00	-0.11
fjs-18	Slate	53	0.22	0.20	0.15	0.11	0.04	0.04	0.06
fjs-16	Sandstone	38	-0.34	-0.38	-0.20	-0.25	-0.12	-0.03	-0.16
fjs-1502	Slate	29	-0.84	-0.65	-0.44	-0.25	-0.02	-0.01	-0.04
fjs-15	Slate	19	0.25	0.11	0.07	-0.06	-0.08	-0.06	-0.12
fjs-17	Slate	46	1.75	1.24	0.87	0.32	-0.08	-0.01	-0.13
fjs-21	Siltstone	8	-0.83	-0.80	-0.51	-0.42	-0.18	-0.08	-0.21

Table S4. THg and Hg isotopic compositions of the Permian E'meishan plume-related mafic rocks from the interior of the Youjiang basin, respectively.

Sample	Type	THg	δ^{202}Hg	δ^{201}Hg	δ^{200}Hg	δ^{199}Hg	Δ^{201}Hg	Δ^{200}Hg	Δ^{199}Hg
ID		ppb	‰	‰	‰	‰	‰	‰	‰
LH 1-1	Dolerite	1.6	-0.67	-0.51	-0.33	-0.14	0.00	0.01	0.03
LH 1-2	Dolerite	2.0	-0.96	-0.72	-0.48	-0.2	0.00	0.01	0.05
LH 1-3	Dolerite	1.6	-1.01	-0.71	-0.48	-0.25	0.04	0.04	0.00
LH 1-4	Dolerite	1.4	-0.85	-0.6	-0.39	-0.13	0.04	0.04	0.06
LH 1-5	Dolerite	1.5	-1.03	-0.7	-0.51	-0.22	0.06	0.01	0.04
DH 1-1	Dolerite	0.4	-1.33	-1.1	-0.65	-0.27	-0.10	0.02	0.06
DH 1-2	Dolerite	0.4	-1.28	-1.06	-0.63	-0.26	-0.10	0.01	0.05
DH 1-3	Dolerite	0.3	-1.03	-0.85	-0.47	-0.21	-0.07	0.05	0.05
DH 1-4	Dolerite	2.8	-0.10	-0.05	0.02	-0.02	0.02	0.07	0.01

REFERENCES CITED

Biswas, A., Blum, J.D., Bergquist, B.A., Keeler, G.J., and Xie, Z.Q., 2008, Natural mercury isotope variation in coal deposits and organic soils: Environmental Science & Technology, v. 42, p. 8303–8309.

Estrade, N., Carignan, J., and Donard, O.F., 2010, Isotope tracing of atmospheric mercury sources in an urban area of northeastern France: Environmental Science & Technology, v. 44, p. 6062–6067.

Gehrke, G.E., Blum, J.D., and Meyers, P.A., 2009, The geochemical behavior and isotopic composition of Hg in a mid-Pleistocene western Mediterranean sapropel: Geochimica et Cosmochimica Acta, v. 73, p. 1651–1665.

Meng, M., Sun, R.Y., Liu, H.W., Yu, B., Yin, Y.G., Hu, L.G., Shi, J.B., and Jiang, G.B., 2019, An integrated model for input and migration of mercury in Chinese coastal sediments: Environmental Science & Technology, v. 53, p. 2460–2471.

Yin, R.S., Feng, X.B., and Meng, B., 2013, Stable mercury isotope variation in rice plants (Oryza sativa L.) from the Wanshan mercury mining district, SW China: Environmental Science & Technology, v. 47, p. 2238–2245.

Zhang, H., Yin, R.S., Feng, X.B., Sommar, J., Anderson, C.W.N., Sapkota, A., Fu, X.W., and Larssen, T., 2013, Atmospheric mercury inputs in montane soils increase with elevation: evidence from mercury isotope signatures: Scientific Reports, v. 3, p. 3322.